ELSEVIER

Thin Solid Films 313–314 (1998) 254–258

thin solid films

Surface disorder production during plasma immersion implantation

T. Lohner[a,*], N.Q. Khánh[a], P. Petrik[a], L.P. Biró[a], M. Fried[a], I. Pintér[a], W. Lehnert[b], L. Frey[b], H. Ryssel[b], D.J. Wentink[c], J. Gyulai[a,b]

[a] *Research Institute for Materials Science, P.O. Box 49, H-1525 Budapest, Hungary*
[b] *Fraunhofer-Institut für Integrierte Schaltungen, IIS-B, Schottkystrasse 10, 91058 Erlangen, Germany*
[c] *Faculty of Applied Physics, University of Twente, P.O. Box 217, 7500 AE Enschede, The Netherlands*

Abstract

Comparative investigations were performed using high-depth-resolution Rutherford backscattering (RBS) combined with channeling, spectroellipsometry (SE) and atomic force microscopy (AFM) to analyze surface disorder and surface roughness formed during plasma immersion implantation of silicon (100) substrates in a gas mixture containing PH_3. In order to enhance the sensitivity to the determination of the oxygen content of the surface oxide layer, the 3.05 MeV ($^4He^+$, $^4He^+$) nuclear resonance was used in combination with channeling. For the analysis of SE data we used the method in which an appropriate optical model is assumed and a best fit to the model parameters is obtained (i.e. the thickness of surface oxide and damaged silicon layers and the volume fraction of the components). Evaluation of RBS spectra yields damage profiles consistent with those obtained by SE modelling. © 1998 Elsevier Science S.A.

Keywords: Plasma immersion ion implantation; Spectroellipsometry; Atomic force microscopy; Rutherford backscattering spectrometry; Surface disorder; Surface roughness

1. Introduction

Plasma immersion implantation (PII) [1] is one of the most promising techniques in IC technology for conformal trench doping [2] and for forming shallow junctions [3] owing to its extra low energy and non-line-of-sight features. In PII doping the silicon wafer is immersed in a plasma containing the dopant species, where the ions accelerated by the bias voltage across the ion sheath are implanted into the surface. An important issue in the ion implantation of semiconductors is the generation of crystallographic damage. Little is known about the degree of damage caused by low energy PII. High resolution X-ray diffraction methods have been used by Chapek et al. [4] to characterize boron-doped silicon fabricated using low energy plasma source ion implantation. Their results suggest that doping by plasma source ion implantation is accompanied by a negligible amount of crystallographic damage. Another concern is the surface roughness of the implanted material after PII processing. Si surface roughness after PII may be detrimental to contacts. The roughness of Si substrates and SiO_2 and $CoSi_2$ films before and after PII was characterized by atomic force microscopy by Jones et al. [5]. They have found that the roughness of Si surfaces increases by a factor of 4–5 during PII. Rutherford backscattering spectrometry (RBS) combined with the channeling technique was applied for the determination of the amount of implanted phosphorus and for the investigation of lattice damage [6].

Hydrogen-bombardment-induced structural changes in single-crystal silicon were studied using spectroscopic ellipsometry (SE) and transmission elec-

* Corresponding author. Tel.: +36 1 3959220; fax: +36 1 3959284; e-mail: lohner@ra.atki.kfki.hu

0040-6090/98/$19.00 © 1998 Elsevier Science S.A. All rights reserved
PII S0040-6090(97)00828-6

tron microscopy by Collins et al. [7]. Various degrees of damage and phase mixtures in the layers were identified. It was concluded that ellipsometry can be used effectively as a non-destructive method for analyzing bombardment-induced microstructural changes in silicon.

In this work, comparative investigations were performed using high-depth-resolution RBS combined with channeling, SE and AFM to analyze surface disorder and surface roughness formed during plasma immersion implantation of silicon (100) substrates.

2. Experimental

Single crystal Si wafers (5.1–6.9 Ωcm p-type ⟨100⟩) have been plasma immersion implanted in a modified reactive ion etching chamber using a doping gas of 1% PH_3 diluted in hydrogen with a DC bias voltage of 1000 V. An RF power of 400 W with 13.56 MHz excitation frequency was used to form a plasma at 0.8 mbar gas pressure. The background pressure was 5×10^{-5} mbar. The PII time duration ranged between 7.5 s and 300 s. Because the penetration of the phosphorus ions in this case ($R_p = 3.2$ nm, $\Delta R_p = 1.8$ nm) is comparable with the thickness of the native oxide, samples have been HF-treated and loaded immediately into the plasma chamber for implantation. The wafers were cut into pieces for different studies.

A SOPRA ES4G rotating polarizer spectroscopic ellipsometer was used for SE measurements. Preliminary experiments were made using a rotating polarizer spectroscopic ellipsometer at Twente University.

In order to obtain a cross-check of the results obtained by SE, studies were also performed with AFM and RBS. AFM measurements were made by, in the tapping mode, selecting a scan window size of $1 \times 1\ \mu m^2$. A Nanoscope III Stand Alone microscope was used. An etched Si tip has been used with a resonant frequency of the cantilever of 276 kHz. The radius of curvature of the tip was measured by high resolution SEM to be 30 nm. Because the roughness values are influenced by tip, scan size and scan conditions, the parameters of the measurements were kept the same from sample to sample. Images of 256×256 pixels were acquired at a scan rate of 2 Hz.

After PII the samples were measured by RBS with a 165° detector. In order to enhance the sensitivity to the determination of the oxygen content of the surface oxide layer, the 3.05 MeV ($^4He^+$, $^4He^+$) nuclear resonance was used in combination with channeling [8]. For investigating the damage depth distribution, we applied a 1 MeV He ion beam and a 97° detector (i.e. with a glancing exit angle of 7° to the surface). In this geometry, the depth resolution was better than 5 nm [9]. The RBS spectra were evaluated by the RBX code written by Kótai which can also handle channelled spectra [10].

3. Results and discussion

For the analysis of SE data we applied the method in which an appropriate optical model is assumed and best fit model parameters are obtained (including the thickness of surface oxide and damaged silicon layers and the volume fraction of the different forms of silicon component in the damaged layers) [11]. This technique requires as input the dielectric functions of the components of the multilayer structure. The reference dielectric function for single-crystal Si (c-Si), amorphous Si (a-Si), ion implantation amorphized Si (ia-Si), and fine-grain polycrystalline Si (poly-Si) were obtained from the literature [12–15]. With reference to the work of Aspnes et al. [16], the unbiased estimator (σ) is used to describe the agreement between the experimental data and the spectrum calculated on the basis of a selected optical model with best-fit model parameters.

Table 1 shows a series of attempted one-layer and two-layer optical models for the sample processed for

Table 1
Layer thickness values and compositions extracted from SE data together with the 90% confidence limits and unbiased estimator (σ) for a PII sample processed for 7.5 s. The bulk material is c-Si

Model	Top overlayer		Bottom overlayer		
	Thickness (nm)	Composition	Thickness (nm)	Composition	σ
7.5A	6.7 ± 0.3	Oxide	—	—	0.078
7.5B	6.8 ± 0.1	Oxide	1.2 ± 0.1	ia-Si	0.024
7.5C	6.8 ± 0.08	Oxide	5.0 ± 0.4	poly-Si	0.019
7.5D	7.2 ± 0.08	Oxide	1.5 ± 0.1	a-Si	0.017
7.5E	7.0 ± 2.2	0.19 ± 0.07 c-Si 0.81 ± 0.07 void	—	—	0.059
7.5F	6.3 ± 0.4	0.56 ± 0.02 a-Si 0.44 ± 0.02 void	—	—	0.037
7.5G	5.4 ± 0.2	0.53 ± 0.02 ia-Si 0.47 ± 0.02 void	—	—	0.037

Table 2
Layer thickness values and compositions extracted from SE data together with the 90% confidence limits and unbiased estimator (σ) for a PII sample processed for 300 s. The bulk material is c-Si

Model	Top overlayer		Bottom overlayer		
	Thickness (nm)	Composition	Thickness (nm)	Composition	σ
300A	2.4 ± 0.6	Oxide	—	—	0.110
300B	12.4 ± 0.5	Oxide	1.3 ± 0.5	ia-Si	0.086
300C	12.2 ± 0.4	Oxide	9.4 ± 2.0	poly-Si	0.063
300D	9.1 ± 0.5	Oxide	45.0 ± 2.6	a-Si	0.070
300E	9.6 ± 1.1	0.28 ± 0.05 c-Si 0.72 ± 0.05 void	—	—	0.061
300F	11.1 ± 0.7	0.56 ± 0.02 a-Si 0.44 ± 0.02 void	—	—	0.042
300G	9.9 ± 3	0.51 ± 0.01 ia-Si 0.49 ± 0.01 void	—	—	0.027
300H	9.9 ± 1.7	0.27 ± 0.06 poly-Si 0.73 ± 0.06 void	—	—	0.070
300I	9.8 ± 0.5	0.49 ± 0.03 a-Si 0.51 ± 0.03 void	1.2 ± 0.2	a-Si	0.025
300J	8.7 ± 0.3	0.33 ± 0.03 poly-Si 0.67 ± 0.03 void	6.1 ± 0.6	poly-Si	0.025
300K	8.5 ± 0.4	0.25 ± 0.05 c-Si 0.75 ± 0.05 oxide	—	—	0.070
300L	10.6 ± 0.7	0.52 ± 0.03 a-Si 0.48 ± 0.03 oxide	—	—	0.051
300M	9.8 ± 0.3	0.47 ± 0.02 ia-Si 0.53 ± 0.02 oxide	—	—	0.034
300N	8.5 ± 0.4	0.25 ± 0.07 poly-Si 0.75 ± 0.07 oxide	—	—	0.074

7.5 s. Rows 7.5A, 7.5E, 7.5F, and 7.5G provide results for a single damaged layer (either pure oxide or a combination of different forms of silicon and void). The latter three models represent surface roughness on the c-Si substrate. The possible existence of a damaged layer beneath the surface oxide layer is explored in rows 7.5B, 7.5C, and 7.5D. Models 7.5C and 7.5D both give good fits.

In the case of a PII sample processed for 15 s, the one-layer model representing roughness with components of ia-Si and void and the two layer models describing damaged layer beneath the surface oxide layer give comparable fit quality.

Table 2 displays SE results for a 300-s exposure. Optical models having a roughness layer as the top overlayer show good fits to the experimental data (models 300G, 300I, and 300J).

Fig. 1 shows the agreement between the experimental and calculated data for an HF etched sample and for the samples PII processed for 7.5 s and 300 s in the case of the best fits. Table 3 shows the measured root mean square (RMS) roughness of samples for three different selected areas. The as-received reference sample shows similar RMS data as that reported in [17]. For the case of the HF etched sample and for the ones irradiated with durations of 7.5 s and 15 s, a moderate increase was observed. However, a substantial increase was found for the sample irradiated for 300 s. This coincides with the results of SE modelling, i.e. for 7.5-s PII processing the good fit was given by two-layer optical models and, on the other hand, for 300 s irradiation, models including surface roughness provided better agreement.

Fig. 2 shows channelled backscattering spectra taken at a scattering angle of 165° and using an analyzing beam energy of 3.045 MeV for samples implanted for 15 s and 300 s, respectively. For comparison, a spectrum measured on an unimplanted (HF-etched only) sample is displayed. The implanted P peak is well separated from the Si leading edge. The peaks labeled ‘O’ correspond to $^4He^+$ particles resonantly scattered from oxygen atoms. Table 4 summarizes the amount (areal density) of oxygen and phosphorus atoms in the surface region of the samples. No phosphorus was detected either on the unimplanted

Table 3
Results of AFM measurements (RMS in nm unit) for PII processed Si

Treatment	Window I	Window II	Window III
As-received	0.089	0.087	0.083
HF etching	0.125	0.140	0.115
PII 7.5 s	0.116	0.111	0.119
PII 15 s	0.109	0.104	0.107
PII 300 s	1.420	1.666	1.429

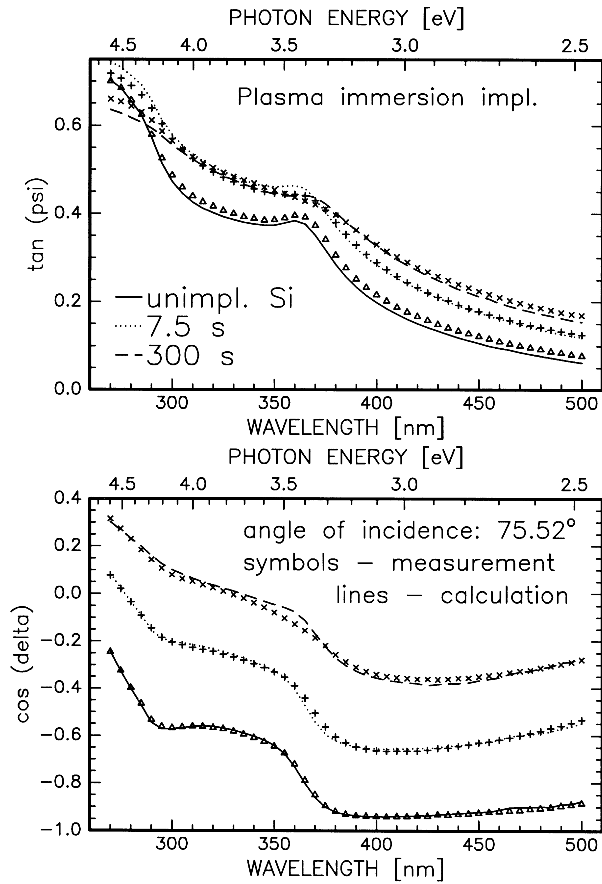

Fig. 1. Experimental and calculated best fit SE spectra for an HF etched Si sample and for the samples PII processed for 7.5 s and 300 s.

or on the 7.5-s implanted sample. Concerning the amount of P, a slight increase for the range of 15–120 s was found, and a decrease was observed for the highest PII duration. More than a factor of five times higher concentration of oxygen was found on samples with exposure times of 7.5–60 s in comparison with an unprocessed surface. We suspect that oxygen was etched from the quartz window of the processing chamber.

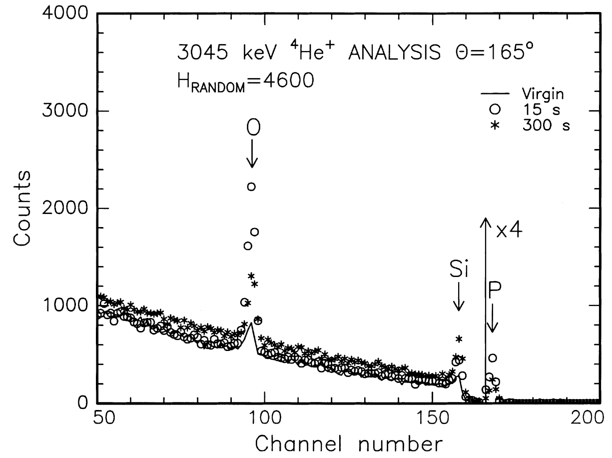

Fig. 2. Backscattering spectra for PII-processed Si taken at a scattering angle of 165° and using an analyzing beam energy of 3045 keV on samples implanted for 15 s and 300 s, respectively. For comparison, a spectrum measured on an unimplanted (HF-etched only) sample is displayed.

All three quantities, the amount of oxygen and P and the damage can be studied using a 1 MeV analyzing beam and glancing detection geometry [9]. Fig. 3 depicts RBS spectra taken at a scattering angle of 97° and using an analyzing beam energy of 1 MeV. For comparison, a spectrum measured on an unimplanted (HF-etched only) sample is displayed. The amount of oxygen and P in the surface layer of the samples extracted from the 1 MeV measurements is given in Table 4. There is good agreement between the results taken at 3.045 MeV and 1 MeV energy. A comparison of the ratio of the amount of oxygen for 7.5 s and for the unimplanted samples both extracted from the 3.045 MeV measurements (~ 6) with the ratio of oxide layer thicknesses (~ 4.5) obtained from the best fit SE evaluations, yields satisfactory agreement. The point defect distribution versus depth obtained by evaluating the RBS data measured at 1 MeV is displayed in Fig. 4. Approximating these distributions with an effective layer thickness we obtain ~ 5 nm,

Table 4
Amount of oxygen and P atoms in PII samples extracted from 3.045 MeV ($^4He^+$, $^4He^+$) nuclear resonance measurements and 3.045 MeV He RBS analysis and 1 MeV He RBS analysis together with the Si/O/P ratio

Implantation time (s)	3.045 MeV nuclear resonance O (10^{16} at./cm^2)	3.045 MeV He RBS P (10^{15} at./cm^2)	1 MeV He RBS O (10^{16} at./cm^2)	1 MeV He RBS P (10^{15} at./cm^2)	1 MeV He RBS Si/O/P
0	0.4 ± 0.05	0	0.52	0	—
7.5	2.4 ± 0.08	< 0.4	2.4	< 0.4	—
15	2.4 ± 0.08	8.3 ± 0.4	2.4	11	0.9/1.6/0.8
30	2.3 ± 0.08	9.2 ± 0.5	—	—	—
60	2.2 ± 0.08	9.9 ± 0.5	—	—	—
120	1.6 ± 0.08	10.0 ± 0.5	1.6	12	1.2/1.7/1.3
300	1.0 ± 0.07	4.0 ± 0.3	0.79	5.2	1.4/1.6/0.8

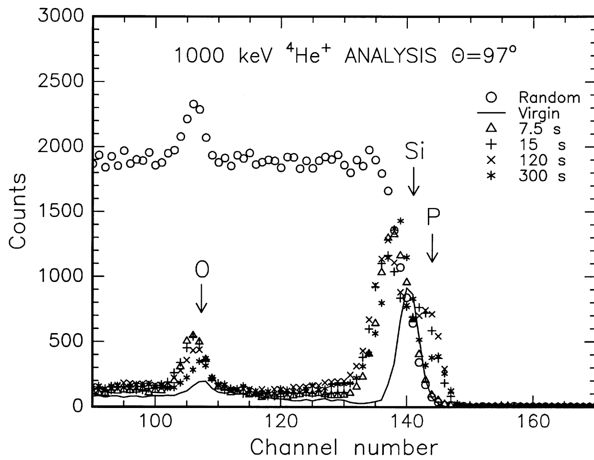

Fig. 3. RBS spectra for PII-processed Si taken at a scattering angle of 97° and using an analyzing beam energy of 1 MeV.

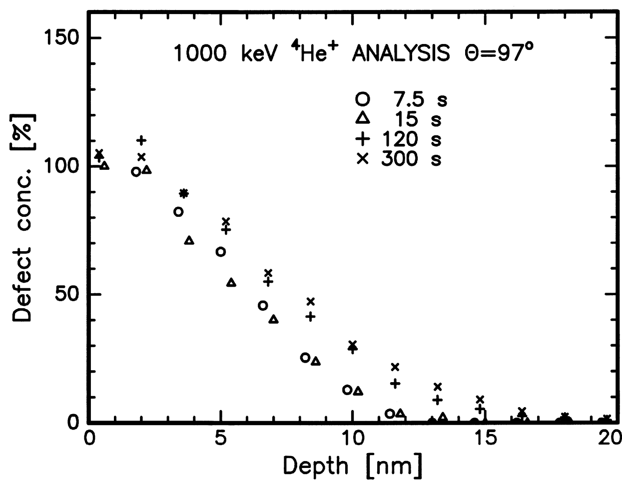

Fig. 4. The point defect distribution versus depth obtained by evaluation of the RBS data measured at 1 MeV for PII-processed Si.

which is in good agreement with the thickness of the bottom poly-Si overlayer for the 7.5 and 300 s samples as extracted from SE data.

4. Conclusion

Analysis of SE data with multilayer optical analysis and the Bruggeman effective medium approximation was used for characterization of surface disorder and roughness induced by PII processing. For the initial period of bombardment, the SE data can be well modeled by a structure consisting of an oxide top overlayer and a damaged bottom layer. For prolonged bombardment, the selection of a roughness top overlayer simultaneously describing damage proved to be satisfactory. For prolonged bombardment the existence of the surface roughness layer was supported by AFM observations. The oxide layer thicknesses extracted from SE data and the amount of oxygen atoms on the surface from RBS show reasonable agreement.

Acknowledgements

One of the authors (T.L.) thanks Dr. A.R. Heyd and Professor Emeritus of Physics K. Vedam (from Pennsylvania State University) for their kindness concerning the use of 'Simulation Spectroellipsometric Program' version 4.01.1988. The work was partly supported by OTKA Grants No. 017344 and 016821. Support from Hungarian–German Intergovernmental Project (Defects in ion implanted silicon, UNG-048-96, TéT, No. D14/96), and EU Copernicus Projects (CIPA CT94.0208 NOCOMO and CIPA-CT94-0131 RESPECT) are greatly appreciated.

References

[1] J.R. Conrad, J. Appl. Phys. 62 (1987) 777.
[2] B. Mizuno, I. Nakayama, N. Aoi, M. Kubota, T. Komeda, Appl. Phys. Lett. 53 (1988) 2059.
[3] X.Y. Qian, N.W. Cheung, M.A. Lieberman, et al., Nucl. Instr. Methods B 55 (1991) 821.
[4] D.L. Chapek, J.R. Conrad, R.J. Matyi, S.B. Felch, J. Vac. Sci. Technol. B 12 (1994) 951.
[5] E.C. Jones, W. En, S. Ogawa, D.B. Fraser, N.W. Cheung, J. Vac. Sci. Technol. B 12 (1994) 956.
[6] N.Q. Khánh, I. Pintér, Cs. Dücsô, et al., Nucl. Instr. Methods Phys. Res. B 112 (1996) 259.
[7] R.W. Collins, B.G. Yacobi, K.M. Jones, Y.S. Tsuo, J. Vac. Sci. Technol. A 4 (1986) 153.
[8] G. Mezey, E. Kótai, P. Révész, et al., Acta Phys. Hung. 58 (1985) 39.
[9] G. Mezey, E. Kótai, T. Lohner, T. Nagy, J. Gyulai, A. Manuaba, Nucl. Instr. Methods 149 (1978) 235.
[10] E. Kótai, Nucl. Instr. Methods Phys. Res. B 85 (1994) 588.
[11] P.J. McMarr, K. Vedam, J. Narayan, J. Appl. Phys. 59 (1986) 694.
[12] D.E. Aspnes, A.A. Studna, Phys. Rev. B 27 (1983) 985.
[13] B.G. Bagley, D.E. Aspnes, A.C. Adams, Bull. Am. Phys. Soc. 25 (1980) 12.
[14] M. Fried, T. Lohner, W.A.M. Aarnink, L.J. Hanekamp, A. van Silfhout, J. Appl. Phys. 71 (1992) 5260.
[15] G.E. Jellison, Jr., M.F. Chisholm, S.M. Gorbatkin, Appl. Phys. Lett. 62 (1993) 3348.
[16] D.E. Aspnes, J.B. Theeten, F. Hottier, Phys. Rev. B 20 (1979) 3292.
[17] L.P. Biró, J. Gyulai, K. Havancsák, A.Yu. Didyk, S. Bogen, L. Frey, Phys. Rev. B 54 (1996) 11853.